Available online at www.sciencedirect.com
ScienceDirect
Trans. Nonferrous Met. Soc. China 31(2021) 475−484
Transactions of Nonferrous Metals Society of China
www.tnmsc.cn

Microstructure and mechanical properties of CuAgZn/GH909 diffusion bonded joint fabricated by hot isostatic pressing

Yi XIAO, Li-hui LANG, Wen-cai XU

School of Mechanical Engineering and Automation, Beihang University, Beijing 100191, China

Received 29 March 2020; accepted 12 October 2020

Abstract: The hot isostatic pressing-diffusion bonding (HIP-DB) was proposed to achieve the joining of CuAgZn and GH909 directly without an interlayer. The microstructure of joint was characterized by scanning electron microscope (SEM), energy dispersive spectrometer (EDS) and X-ray diffraction (XRD). The microhardness and shear strength were tested to investigate the mechanical properties of joint. The results showed that the interface was complete, and the joint was compact, uniform and free of unbonded defects. The maximum microhardness of joint was HV 443, higher than that of two base alloys, and the average shear strength of joint reached 172 MPa. It is concluded that a good metallurgical bonding between CuAgZn and GH909 can be obtained by HIP-DB with the process parameters of 700 °C,150 MPa and 3 h.

Key words: CuAgZn alloy; GH909 superalloy; diffusion bonding; hot isostatic pressing

1 Introduction

CuAgZn alloy consisting of copper, silver and zinc is a Cu-based alloy, which has the features of low melting point, good fluidity and wettability. GH909 superalloy is a new kind of Fe−Ni−Co based superalloy with low thermal expansion, high strength and plasticity, high thermal fatigue resistance, low expansion coefficient and other comprehensive mechanical properties [1]. The joining of CuAgZn and GH909 these two new alloys can perform a high integrated property. However, the bonding of dissimilar materials such as CuAgZn alloy and GH909 superalloy has always been a challenging work due to the large differences in the thermal expansion coefficient and elemental composition. One important application of hot isostatic pressing (HIP) is an interfacial bonding by using a high flexible media pressure loading at a high elevated temperature [2]. Therefore, the hot isostatic pressing-diffusion bonding (HIP-DB) method is an innovative joining technology using a multiplier effect of high temperature and high pressure to bond similar or dissimilar materials which are difficult to be bonded by other methods [3]. Especially, the pressure of hot isostatic pressing-diffusion bonding is applied with a gas (usually inert gas), hence it is flexible and isostatic [4]. Consequently, with the characteristics of three-dimensional isotropic and flexible medium applied pressure, the joints obtained by hot isostatic pressing-diffusion bonding have less residual stress, less welding deformation and better quality.

Until now, few studies have been done on the joining of CuAgZn alloy and GH909 superalloy as they are both novel materials. Cu−Ag−Zn alloys are often reported as filler metals to braze materials [5−7] rather than the base materials. Especially, many researchers address to apply Cu−Ag−Zn or Cu−Ag alloys as solders to braze superalloys with superalloys [8,9], metals [10],

Corresponding author: Li-hui LANG; Tel: +86-18911301187; E-mail: lang@buaa.edu.cn
DOI: 10.1016/S1003-6326(21)65510-3

cermets [11], ceramics [12] and composites [13]. The studies of the joining of GH909 superalloy mainly focus on laser welding [14−18]. And more studies for the diffusion bonding of copper or Cu-based alloys to superalloys directly [19] or as intermediate layers [20,21] were carried out. Regarding to the hot isostatic pressing-diffusion bonding of superalloys, some studies have been conducted [22−24]. But the practical application of hot isostatic pressing- diffusion bonding is more in the joining of metals or alloys in the field of nuclear [25,26], typical joints like W/steel [27], W/CuCrZr [28], steel/steel [29], steel/CuCrZr [30], Be/steel [31], and Be/CuCrZr [32], etc. As described above, little attention has been focused on the joining of CuAgZn alloy and GH909 superalloy.

In the present work, a method was proposed to use hot isostatic pressing to realize the diffusion bonding of the CuAgZn alloy and the GH909 superalloy in the solid state directly without an interlayer. The microstructure, element distribution, phase composition and mechanical properties of the CuAgZn/GH909 diffusion bonded joint were studied. The purpose of this work is to provide a feasible method for the direct bonding of CuAgZn alloy and GH909 superalloy.

2 Experimental

2.1 Materials

The experimental CuAgZn alloy was cast with the Cu to Ag to Zn mass ratio of 50:25:25. The chemical composition of the experimental GH909 superalloy is given in Table 1. The material of the capsule used in this experiment was oxygen-free copper and the capsule was processed to cover the two base alloys for vacuum purpose. The oxygen-free copper capsule was employed as it possessed good plasticity and low yield strength at a high temperature, which would promote the pressure transfer and the diffusion bonding of the two base alloys.

Table 1 Chemical composition of experimental GH909 superalloy (wt.%)

Ni	Co	Nb	Ti	Cr	Cu
35.0	14.0	4.3	1.5	0.5	0.5
Mn	Si	Al	Others	Fe	
0.45	0.3	0.1	0.07	Bal.	

2.2 Procedure

Firstly, the bonded surfaces of the base alloys were ground and polished to remove the oxide layer and enhance the surface roughness, then ultrasonic cleaner was applied to cleaning the residual oil remained on the surfaces. Subsquently, the two base alloys were assembled into the oxygen-free copper capsule as shown in Fig. 1, and then the capsule was degassed until the vacuum degree reached 1.0×10^{-3} Pa and sealed in vacuum state. Finally, hot isostatic pressing was carried out to make a diffusion bonding of the CuAgZn alloy and the GH909 superalloy under the process parameters of 700 °C, 150 MPa and 3 h of holding time. After hot isostatic pressing, the capsule was removed by machining.

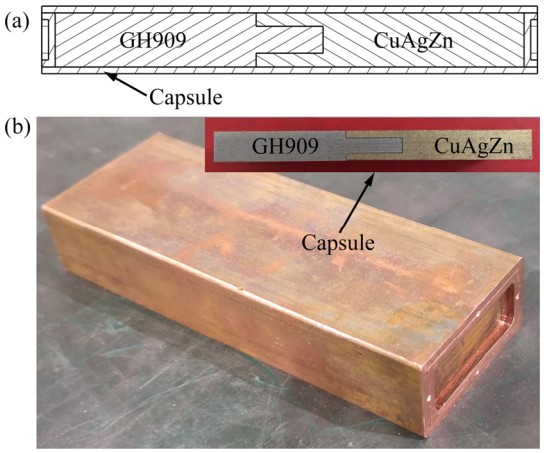

Fig. 1 Assembled samples: (a) Schematic diagram of assembled sample; (b) Picture of assembled sample

2.3 Methods

The microstructure and fracture morphologies of the CuAgZn/GH909 bonded joint were observed by a JSM6010 scanning electron microscope (SEM). The element distribution of the joint was analyzed by a CamScan−3400 energy dispersive spectrometer (EDS). The sample was cut, ground and polished before SEM and EDS. The phase composition of the joint was characterized by a D/MAX−2500 X-ray diffraction (XRD). Three shear samples were prepared, as shown in Fig. 2, and the shear tests were conducted by a CTM100G electronic universal testing machine. Three microhardness samples were prepared, and the FM800 Vickers hardness tester was applied to testing the microhardness of the joint with a load of 1.96 N for 15 s. Three points for each position were evaluted to determine a average value.

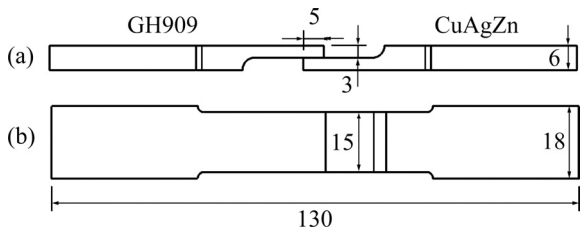

Fig. 2 Schematic diagram of shear sample (unit: mm): (a) Front view; (b) Top view

3 Results and discussion

3.1 Microstructure of CuAgZn/GH909 joint

The microstructure of the CuAgZn/GH909 diffusion bonded joint is shown in Fig. 3. The bonded joint can be divided into three regions as shown in Fig. 3(a), in which the areas from left to right are GH909 base alloy region, bonded interface and CuAgZn base alloy region, respectively. It can be found that the bonded interface is tight and complete, and the joint is compact, uniform and free of unbonded defects such as cracks, pores and voids, which can indicate that a good metallurgical bonding between the CuAgZn alloy and the GH909 superalloy is obtained. The desirable joining results for these two dissimilar materials benefit from the multiplier effect of high temperature and isostatic pressure of hot isostatic pressing-diffusion bonding. During the hot isostatic pressing-diffusion bonding process, on one hand, pores and voids were gradually eliminated by the high flexible media pressure. On the other hand, atoms in two base alloys interdiffused across the interface at the high temperature. Therefore, a smooth transition of the interfacial components was achieved and a sound joint was obtained. In addition, the segregation of Ag element in the CuAgZn base alloy can be clearly observed.

The magnified image of Fig. 3(a) is shown in Fig. 3(b). There is a diffusion layer at the interface as shown in Region I in Fig. 3(b), but it is not distinct. The magnified image of Region I was obtained as shown in Fig. 3(c), and it can be found that the thickness of the diffusion layer is approximately 3 μm, which is relatively thin. The main reason for the formation of the diffusion layer is that the intermetallic compounds (IMCs) were formed at the interface by the interdiffusion and reaction of the atoms in the two base alloys [33]. When dissimilar materials are joined together by diffusion bonding process, the growth of the interfacial reaction layer, particularly the thickening of the intermetallic compounds reaction layer is detrimental to the joint properties [34]. Because the interfacial reaction layer is prone to defects and becomes the preferential layer to crack [35], the

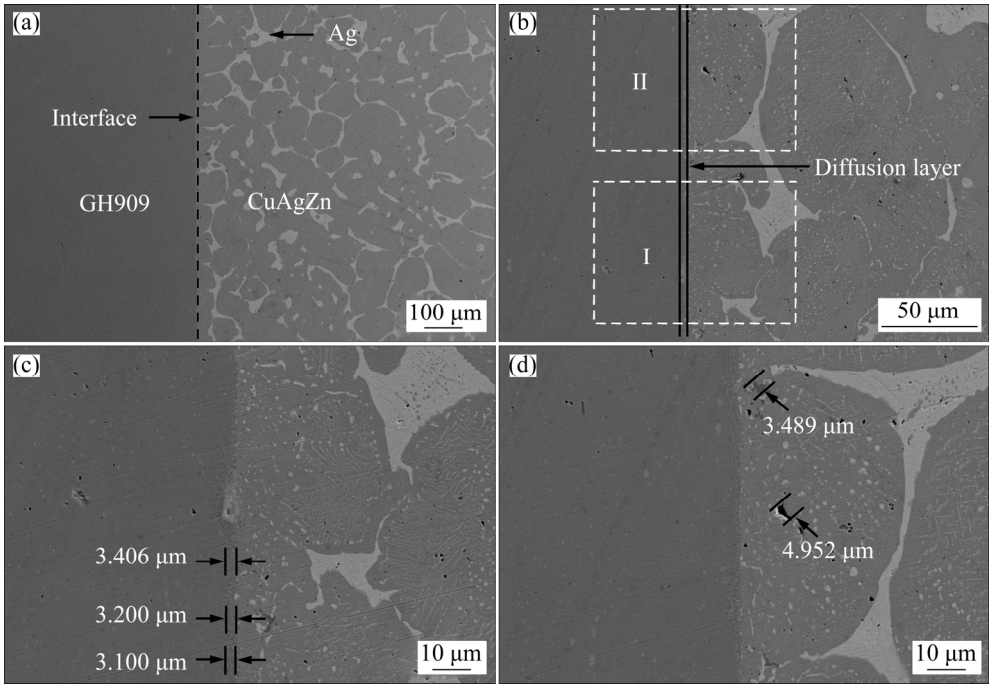

Fig. 3 SEM micrographs of cross section of CuAgZn/GH909 bonded joint: (a) Morphology of whole joint; (b) Magnified image of (a); (c) Magnified image of Region I in (b); (d) Magnified image of Region II in (b)

excessive thickening of the diffusion layer will be harmful to the joint properties [36]. Moreover, the study [37] has shown a linear relationship between the thickness of the diffusion layer and the square root of the holding time, as shown in the following equation:

$$\chi \propto \sqrt{Dt} \quad (1)$$

where x is the thickness of the diffusion layer (m); D is the diffusion coefficient (m^2/s) related to the temperature; t is the holding time (s). It can be concluded from Eq. (1) that the temperature and holding time selected for this experiment were suitable, and there was no severe interfacial reaction and no excessive increase in the thickness of the diffusion layer.

Another key point is that the microvoids are observed in CuAgZn base alloy near the interface as shown in Region II in Fig. 3(b). From the magnified image Fig. 3(d) of Region II, the maximum size of the microvoids is no more than 5 μm. Conversely, there are no microvoids in GH909 base alloy, and it can be inferred that these microvoids may result from the Kirkendall effect due to the unbalanced diffusion.

3.2 Element distribution of CuAgZn/GH909 joint

The element distribution of the CuAgZn/GH909 diffusion bonded joint was studied by using line scanning analysis of EDS as shown in Fig. 4 and the result shows that there is significant element diffusion across the interface. The Fe, Ni and Co elements in the GH909 base alloy and Cu, Ag and Zn elements in CuAgZn base alloy interdiffuse across the interface, which can indicate that there is a diffusion zone in both GH909 and CuAgZn base alloys. Furthermore, the segregation of Ag element in the CuAgZn base alloy can also be clearly observed in Fig. 4. The elemental analysis was performed at three points, as shown in Fig. 4, and Point 1 was in GH909 base alloy region 50 μm from the interface, Point 2 was at the bonded interface, and Point 3 was in CuAgZn base alloy region 50 μm from the interface. The corresponding analysis results are displayed in Table 2. Cu is detected at Point 1 and Ni is detected at Point 3, which can confirm that there is sufficient element diffusion between the two base alloys. In addition, at Point 2 at the interface, the content of Fe in GH909 base alloy is the highest, followed by Co and Ni. The content of Cu in CuAgZn base alloy is the highest, followed by Zn and Ag. This result shows the diffusion fluxes of the main elements in the two base alloys at the interface.

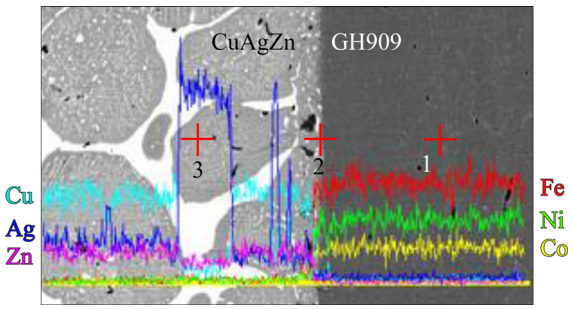

Fig. 4 Line scanning analysis of EDS for CuAgZn/GH909 bonded joint

Table 2 EDS results for CuAgZn/GH909 bonded joint (at.%)

Element	Point 1	Point 2	Point 3
Fe	43.28	44.45	–
Ni	34.69	3.55	1.6
Co	13.39	13.11	–
Cu	2.56	20.08	64.49
Ag	–	3.21	7.26
Zn	–	8.59	26.65
Nb	2.93	3.68	–
Ti	1.81	1.7	–
Si	0.87	0.89	–
Cr	0.47	0.74	–
Total	100	100	100

3.3 Mechanical properties of CuAgZn/GH909 joint

The mechanical properties of CuAgZn alloy should be investigated to be compared with the CuAgZn/GH909 bonded joint because the microhardness and shear strength of GH909 base alloy are higher than those of CuAgZn base alloy. Since the CuAgZn alloy is a kind of new material which lacks relevant mechanical properties data, the microhardness and shear strength of the CuAgZn base alloy employed in this experiment were directly tested, and the results are shown in Tables 3 and Table 4.

Table 3 Microhardness of CuAgZn base alloy

Number	Microhardness (HV)
1	105.5
2	105.5
3	108
4	106
5	103.2
6	107
Average	105.9

Table 4 Shear strength of CuAgZn base alloy

Number	Shear strength/MPa
1	229.2
2	234.6
3	226.8
4	230.4
5	219.6
6	225
Average	227.6

The microhardness from the GH909 superalloy side to the CuAgZn alloy side was measured. The location of the measured points and the distribution of the microhardness are shown in Fig. 5. On the whole, the microhardness decreases slightly from the interface to the base alloy on both sides with the increase of distance. Because the interfacial diffusion layer is mainly composed of intermetallic compounds and solid solutions, it exhibits higher microhardness than the two base alloys. When crossing the interface, the microhardness is steeply decreased from the range of the hot isostatic pressing-diffusion bonded (HIP-DBed) GH909 superalloy to the range of the HIP-DBed CuAgZn alloy. Especially, on the GH909 alloy side, the maximum microhardness is HV 443, which is located near the interface. The farther the distance from the interface, the lower the microhardness, and finally, the stable value HV 431 can be obtained, which can be decided as the microhardness of the HIP-DBed GH909 superalloy. The microhardness is much higher than that of the GH909 base superalloy before HIP-DB (HV 208) and the GH909 laser-welded joint (HV 250) [38]. It can be found that GH909 superalloy has been hardened after HIP-DB process. On the CuAgZn side, the distribution of microhardness is similar to that of the GH909 superalloy side. The maximum microhardness of HV 114 is also located near the interface, and the stable value HV 106 is obtained, which is within the range of the CuAgZn base alloy before HIP-DB process. And it can be seen that the microhardness of CuAgZn alloy does not change significantly after the HIP-DB process, which is different from the variation of the GH909 superalloy.

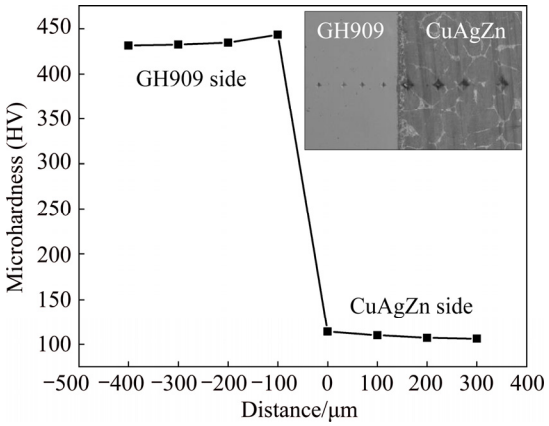

Fig. 5 Location of measured points and microhardness distribution of joint

The measured shear strength of the CuAgZn/GH909 bonded joint is shown in Table 5. The average shear strength of the joint reaches 172 MPa, which is as high as 76% that of the CuAgZn base alloy, and this value is relatively high in the absence of an intermediate layer.

Table 5 Shear strength of CuAgZn/GH909 bonded joint

Number	Shear strength/MPa
1	165.552
2	170.001
3	180.016
Average	171.856

3.4 Shear fracture of CuAgZn/GH909 joint

The fracture morphology of the shear specimen is shown in Fig. 6. The fracture region forms on the CuAgZn alloy side near the interface because the interfacial shear strength is the lowest and some microvoids caused by the Kirkendall effect exist on the CuAgZn alloy side. The fracture on the CuAgZn alloy side has obvious plastic deformation and necking phenomenon, and the length of the fracture is extended from 5 to 6 mm. On the contrary, the fracture on the GH909 alloy side has no deformation or elongation. It can be

seen that the experimental shear stress causes plastic deformation of the CuAgZn base alloy, but has not yet reached the plastic deformation range of the GH909 base alloy. The fractures on both sides are flat and bright, and the parallel lines can be observed. It can be found that the shear fracture is mainly characterized by brittle fracture. The shear fracture morphologies were further observed by SEM, and the results are shown in Fig. 7.

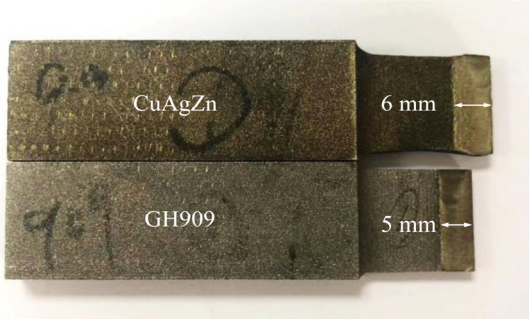

Fig. 6 Fracture morphologies of shear samples

In Fig. 7(a), the shear fracture is flat and bright, and obviously, there is a crack formation (Region I), a crack propagation (Region II) and a shear lip (Region III). In the magnified image of Fig. 7(a) as shown in Fig. 7(b), there are flat parallel lines at the fracture (Area IV), which can be determined that these areas are brittle. In addition, there are tearing edges and a certain number of dimples at the fracture (Area V), which can be determined that these areas are ductile. Typical brittle areas and ductile areas are shown in Figs. 7(c) and (d), respectively. Therefore, the shear fracture has the common characteristics of both brittle fracture and ductile fracture, and it is characterized by the ductile−brittle mixed fracture morphology and exhibits micro-plasticity. However, the brittle fracture areas are significantly more than the ductile fracture areas in general, and the ductile characteristics are not more obvious compared to the brittle characteristics. Hence the shear fracture is mainly characterized by brittle fracture, which is consistent with the observation of the macroscopic morphology.

With further higher magnification observation, as shown in Fig. 8, there are a large number of cleavage steps and river-like patterns (rectangular areas in Figs. 8(a), (b), (c) and (d)) at the fracture, and small, shallow dimples and tearing edges (circular areas in Figs. 8(a), (b), (c) and (d)) exist at the intersection of the steps, which can indicate that these steps were formed by tearing. According to the fracture mechanism, it is speculated that the quasi-cleavage fracture occurred. The fracture process was analyzed, with the increase of shear stress, plastic deformation firstly occurred in the

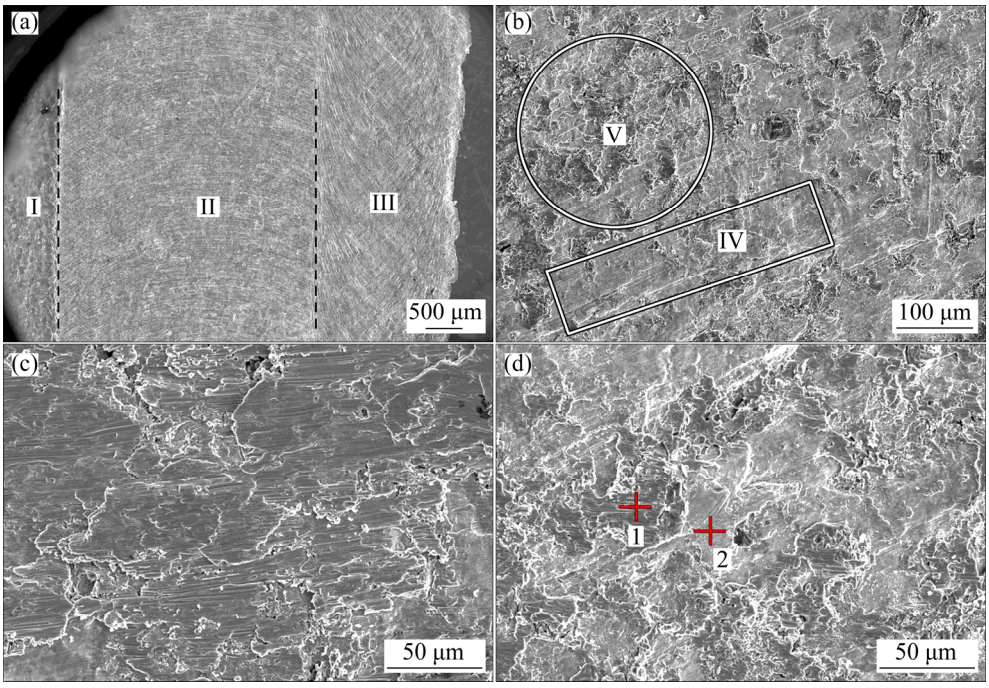

Fig. 7 SEM micrographs of shear fracture of CuAgZn/GH909 bonded joint: (a) Morphology of whole fracture; (b) Magnified image of (a); (c) Characteristic of brittle fracture; (d) Characteristic of ductile fracture

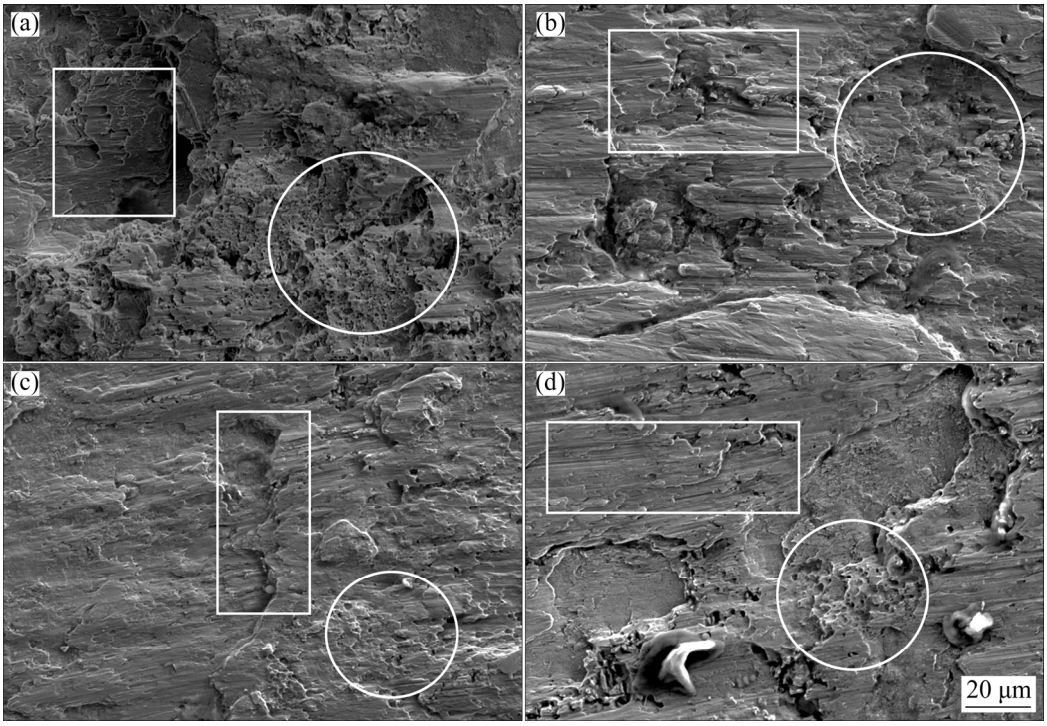

Fig. 8 SEM micrographs of shear fracture in four regions: (a) Region 1; (b) Region 2; (c) Region 3; (d) Region 4

CuAgZn base alloy (Region I in Fig. 7(a)). While the joint was brittle and cannot coordinate the plastic deformation of the CuAgZn base alloy. And due to the microvoids caused by the Kirkendall effect, stress concentration increased on the CuAgZn alloy side near the interface. When the stress concentration reached the critical value, cracks were formed and rapidly propagated in Region II in Fig. 7(a). Finally, the shear sample fractured in Region III in Fig. 7(a). This fracture process was similar to that of quasi-brittle fracture.

The EDS analysis was performed on two points (Fig. 7(d)) at the fracture, and Point 1 was in the ductile area and Point 2 was in the brittle area. The EDS analysis results are shown in Table 6. At Point 1, the main elements are Cu and Zn, where ductile phases may be formed by these elements. At Point 2, the main elements are Ag, Zn and Fe, where brittle phases may be formed by these elements. Therefore, it can be considered that the different elements in the two base alloys interdiffused to form various phases during the hot isostatic pressing-diffusion bonding process, and the shear fracture exhibits different characteristics due to these phases.

Table 6 EDS results for shear fracture (at.%)

Point	Fe	Co	Ni	Cu	Zn	Ag	Total
1	2.16	0.77	2.07	67.88	22.93	4.19	100
2	11.22	7.73	1.38	9.73	13.07	56.87	100

In order to analyze the phase composition more accurately and verify the analysis results of EDS, X-ray diffraction analysis which employed a Cu target with 40 kV voltage and 200 mA current was used to analyze the phase composition of the fracture. The results of XRD are shown in Fig. 9, the main phases at the fracture are Ag (solid solution), $Cu_{0.64}Zn_{0.36}$ and Fe_3Zn_{10}. Among them, Fe_3Zn_{10} is a Fe−Zn intermetallic compound while Ag is a solid solution, and they are both brittle phases, which results in the brittle characteristics of the shear fracture. $Cu_{0.64}Zn_{0.36}$ is a Cu−Zn eutectic phase, and it is an electronic compound that belongs to a high-strength plastic phase, which results in the ductile characteristics of the shear fracture. The results are consistent with the previous analysis based on the EDS. The fracture in this work is different from the ductile fracture of the superalloy joint brazed by CHEN et al [39] using the copper foil because the Ag and Zn elements in the CuAgZn alloy also affect the joint properties. More specifically, for the joining of superalloys, Cu can restrain the formation of intermetallics [40] and

decrease the formation of brittle phases [41], and Ag forms a solid solution which is brittle [42] while the solid solution can enhance the joint microhardness [43]. SIMOES et al [44] also used Ag−Cu sputtered-coated Ti foil to increase the hardness and eliminate the detrimental extensive segregation of hard and brittle compounds, which ultimately improved the mechanical properties of joints. Consequently, it can be confirmed that the diverse elements in the two base alloys reacted and formed Fe−Zn, Cu−Zn intermetallic compounds and Ag solid solution in the diffusion zone during the hot isostatic pressing-diffusion bonding process. Fe−Zn intermetallic compound and Ag solid solution are brittle phases, and they enhanced the joint microhardness while decreased the joint strength. Cu−Zn intermetallic compound is a ductile phase, and it reduced the brittleness of the joint.

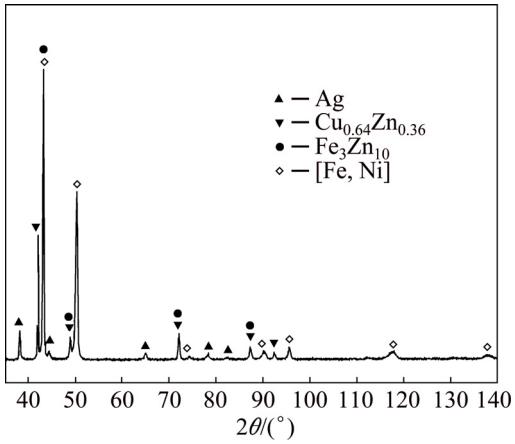

Fig. 9 XRD pattern of shear fracture

4 Conclusions

(1) The CuAgZn alloy and GH909 superalloy were directly diffusion bonded by hot isostatic pressing successfully with the process parameters of 700 °C, 150 MPa and 3 h. The bonded interface was tight and complete, and the joint was compact, uniform and free of unbonded defects. The diffusion layer at interface was not distinct and the thickness was approximately 3 μm, which was beneficial to the properties of the joint. There was significant interdiffusion across the interface at the joint and the diffusion zone existed in both GH909 and CuAgZn base alloys.

(2) The joint exhibited higher microhardness than the two base alloys and the maximum microhardness was HV 443, which was attributed to the higher microhardness intermetallic compounds and solid solutions formed in the diffusion zone. The average shear strength of the joint reached 172 MPa, which was as high as 76% that of the CuAgZn base alloy.

(3) The brittle nature dominated the shear fracture, but it also had ductile characteristics as Fe−Zn, Cu−Zn intermetallic compounds and Ag solid solution were formed in the diffusion zone. These brittle and ductile phases together affected the fracture characteristics.

Acknowledgments

The authors are grateful for the financial support from the Advanced Space Propulsion Technology Laboratory Open Fund, China (LabASP-2018-16).

References

[1] LUO Ming, LI Hai-zhen. On the machinability and surface finish of superalloy GH909 under dry cutting conditions [J]. Materials Research, 2018, 21(4): 1−8.

[2] GEAMAN V, AXENTE M. Applications of hot isostatic processing for high performance aluminum castings [J]. Metalurgia International, 2009, 14: 95−98.

[3] AXENTE M, GEAMAN V. A short lookaround in the field of isostatic processing [J]. Metalurgia International, 2009, 14: 119−122.

[4] ATKINSON H V, DAVIES S. Fundamental aspects of hot isostatic pressing: An overview [J]. Metallurgical and Materials Transactions A, 2000, 31(12): 2981−3000.

[5] HASANABADI M, SHAMSIPUR A, NAJAFI SANI H, OMIDVAR H, SAKHAEI S. Interfacial microstructure and mechanical properties of tungsten carbide brazed joints using Ag−Cu−Zn plus Ni/Mn filler alloy [J]. Transactions of Nonferrous Metals Society of China, 2017, 27(12): 2638−2646.

[6] ZHANG Li-xia, ZHANG Chi-ping, FENG Ji-cai. Numerical simulation of TiC cermet/iron joint brazed with Ag−Cu−Zn filler metal [J]. Transactions of Nonferrous Metals Society of China, 2005, 15(S2): s30−s34.

[7] LI Zhuo-ran, FENG Ji-cai, CAO Jian. Vacuum brazing of TiB_2 cermet to TiAl-based alloys using Ag−Cu−Zn filler metal [J]. Transactions of Nonferrous Metals Society of China, 2003, 13(S1): s39−s41.

[8] KHORRAM A, GHOREISHI M, TORKAMANY M J, BALI M M. Laser brazing of Inconel 718 alloy with a silver based filler metal [J]. Optics and Laser Technology, 2014, 56: 443−450.

[9] KHORRAM A, GHOREISHI M. Comparative study on laser brazing and furnace brazing of Inconel 718 alloys with silver based filler metal [J]. Optics and Laser Technology, 2015, 68: 165−174.

[10] REN H S, XIONG H P, LONG W M, SHEN Y X, PANG S J, CHEN B, CHENG Y Y. Interfacial diffusion reactions and mechanical properties of Ti_3Al/Ni-based superalloy joints brazed with AgCuPd filler metal [J]. Materials Characterization, 2018, 144: 316−324.

[11] ZHANG Li-xia, LEI Min, YANG Zhi-ye, FENG Ji-cai. Interfacial microstructure and properties of TiC cermet and GH3128 joint brazed using AgCuNiLi [J]. Rare Metal Materials and Engineering, 2017, 46(11): 3410−3415. (in Chinese)

[12] SONG Yan-yu, LIU Duo, HU Sheng-peng, SONG Xiao-guo, LEI Yu-zhen, CAO Jian. Brazing of metallized SiC ceramic to GH99 superalloy using graphene nanoplatelets reinforced AgCuTi composite filler [J]. Ceramics International, 2019, 45(7): 8962−8970.

[13] GUO Wei, GAO Teng-fei, CUI Xue-fei, ZHU Ying, CHU P K. Interfacial reactions and zigzag groove strengthening of C/C composite and Rene N5 single crystal brazed joint [J]. Ceramics International, 2015, 41(9): 11605−11610.

[14] YAN Fei, ZHAN Tao, LIU Sang, ZHU Zheng-wu, WANG Chun-ming, HU Xi-yuan. Study on softening behavior of laser welded joint in GH909 alloy [J]. Journal of Mechanical Science and Technology, 2017, 31(11): 5459−5465.

[15] YAN Fei, HU Chong-jing, ZHANG Xiong, CAI Yuan-zheng, WANG Chun-ming, WANG Jun, HU Xi-yuan. Influence of heat input on HAZ liquation cracking in laser welded GH909 alloy [J]. Optics and Laser Technology, 2017, 92: 44−51.

[16] YAN Fei, LIU Sang, HU Chong-jing, WANG Chun-ming, HU Xi-yuan. Liquation cracking behavior and control in the heat affected zone of GH909 alloy during Nd: YAG laser welding [J]. Journal of Materials Processing Technology, 2017, 244: 44−50.

[17] LIU Ting, YAN Fei, LIU Sang, LI Ruo-yang, WANG Chun-ming, HU Xi-yuan. Microstructure and mechanical properties of laser-arc hybrid welding joint of GH909 alloy [J]. Optics and Laser Technology, 2016, 80: 56−66.

[18] YAN Fei, WANG Chun-ming, WANG Ya-jun, HU Xi-yuan, WANG Tian-jiao, LI Jian-min, LI Guo-zhu. A study of the mechanism of laser welding defects in low thermal expansion superalloy GH909 [J]. Materials Characterization, 2013, 78: 21−30.

[19] LI Peng, LI Jing-long, XIONG Jiang-tao, ZHANG Fu-sheng, LIANG Li. Investigations on interface microstructure and strength properties of dissimilar tin bronze/superalloy diffusion bonded joints [J]. Science and Engineering of Composite Materials, 2015, 22(5): 511−515.

[20] REN H S, REN X Y, XIONG H P, LI W W, PANG S J, USTINOV A I. Nano-diffusion bonding of Ti_2AlNb to Ni-based superalloy [J]. Materials Characterization, 2019, 155: 1−11.

[21] QI Xian-sheng, XUE Xiang-yi, TANG Bin, KOU Hong-chao, HU Rui, LI Jin-shan. Phase evolution of diffusion bonding interface between high Nb containing TiAl alloy and Ni−Cr−W superalloy [J]. Rare Metal Materials and Engineering, 2015, 44(7): 1575−1580. (in Chinese)

[22] YAO Yao, YE Jian-shui, DONG Jian-xin, YAO Zhi-hao, ZHANG Mai-cang, GUO Wei-min. Elements diffusion law of DD407/FGH95 diffusion bonding under hot isostatic pressure I. Building diffusion bonding model [J]. Acta Metallurgica Sinica, 2013, 49(9): 1041−1050. (in Chinese)

[23] YAO Yao, DONG Jian-xin, YAO Zhi-hao, ZHANG Mai-cang, GUO Wei-min. Elements diffusion law of DD407/FGH95 diffusion bonding under hot isostatic pressure II. Model verification and experimental analysis [J]. Acta Metallurgica Sinica, 2013, 49(9): 1051−1060. (in Chinese)

[24] YAN Lai-cheng, YAN Ping, ZHAO Jing-chen. Microstructure and properties of diffusion couple of superalloy bonded by HIP [J]. Journal of Iron and Steel Research, 2012, 24(1): 48−53. (in Chinese)

[25] YANG Fa-zhan, SHEN Li-ru, JIN Fan-ya, XU Ze-jin, DONG Yu-ying. Effects of hot isostatic pressing joining temperature on copper coating as the interlayer [J]. Rare Metal Materials and Engineering, 2017, 46(12): 3972−3976. (in Chinese)

[26] JUNG Y I, PARK J Y, CHOI B K, LEE J S, KIM H G, PARK D J, PARK J H, KIM S K, LEE D W, CHO S. Activities of HIP joining of plasma-facing armors in the blanket first-wall in Korea [J]. Fusion Engineering and Design, 2016, 109: 448−453.

[27] LIU Wen-sheng, PANG Xin-kuan, CAI Qing-shan, MA Yun-zhu, ZHU Wen-tan. Fabrication of W/steel joint using hot isostatic pressing with Ti/Cu/Ti liquid forming interlayer [J]. Fusion Engineering and Design, 2018, 135: 59−64.

[28] BANG E, CHOI H, KIM H C, KIM K, HONG S H. Manufacturing and testing of flat type W/Cu/CuCrZr mock-ups by HIP process with PVD coating [J]. Fusion Engineering and Design, 2019, 146(SI): s603−s608.

[29] WAKUI T, ISHII H, NAOE T, KOGAWA H, HAGA K, WAKAI E, TAKADA H, FUTAKAWA M. Optimum temperature for HIP bonding invar alloy and stainless steel [J]. Materials Transactions, 2019, 60(6): 1026−1033.

[30] ORDAS N, SAMANIEGO F, ITURRIZA I, GOMEZ A, ESCUDERO C, FERNANDEZ-CALVO A I, COBO I, BANETTA S, HEIKKINEN S, CICERO T. Mechanical and microstructural characterization of HIP joints of a simplified prototype of the ITER NHF first wall panel [J]. Fusion Engineering and Design, 2017, 124: 999−1003.

[31] HUNT R M, GOODS S H, YING A, DORN C K, ABDOU M. Diffusion bonding beryllium to reduced activation ferritic martensitic steel: Development of processes and techniques [J]. Fusion Engineering and Design, 2012, 87(9): 1550−1557.

[32] YE Lin-sen, CHEN Ji-ming, XIE Dong-hua, WANG Xi-sheng, XU Ze-jin, CHEN Wei. Study on interface behavior of Be/CuCrZr alloy by diffusion bonding [J]. Rare Metal Materials and Engineering, 2010, 39(1): 122−125. (in Chinese)

[33] AZIZI A, ALIMARDAN H. Effect of welding temperature and duration on properties of 7075 Al to AZ31B Mg diffusion bonded joint [J]. Transactions of Nonferrous Metals Society of China, 2016, 26(1): 85−92.

[34] BALASUBRAMANIAN M. Development of processing windows for diffusion bonding of Ti−6Al−4V titanium alloy and 304 stainless steel with silver as intermediate layer [J]. Transactions of Nonferrous Metals Society of China, 2015, 25(9): 2932−2938.

[35] DENG Yun-hua, GUAN Qiao, TAO Jun. Effect of heating

time on bonding interface, atom diffusion and mechanical properties of dissimilar titanium joints produced by thermal self-compressing bonding [J]. Transactions of Nonferrous Metals Society of China, 2018, 28(4): 662−668.
[36] LEE K S, KWON Y N. Solid-state bonding between Al and Cu by vacuum hot pressing [J]. Transactions of Nonferrous Metals Society of China, 2013, 23(2): 341−346.
[37] SEYYED AFGHAHI S S, JAFARIAN M, PAIDAR M, JAFARIAN M. Diffusion bonding of Al 7075 and Mg AZ31 alloys: Process parameters, microstructural analysis and mechanical properties [J]. Transactions of Nonferrous Metals Society of China, 2016, 26(7): 1843−1851.
[38] WANG Chun-ming, CAI Yuan-zheng, HU Chong-jing, ZHANG Xiong, YAN Fei, HU Xi-yuan. Morphology, microstructure, and mechanical properties of laser-welded joints in GH909 alloy [J]. Journal of Mechanical Science and Technology, 2017, 31(5): 2497−2504.
[39] CHEN W S, WANG C Y, SHIUE R K. Brazing Inconel 625 using the copper foil [J]. Metallurgical and Materials Transactions A, 2013, 44(13): 5724−5731.
[40] ZHANG Feng, WANG Ting, JIANG Si-yuan, ZHANG Bing-gang, FENG Ji-cai. Microstructural characteristics and mechanical properties of an electron beam-welded Ti/Cu/Ni joint [J]. Journal of Materials Engineering and Performance, 2018, 27(5): 2354−2363.
[41] CAI Xiao-long, SUN Da-qian, LI Hong-mei, MENG Chao, WANG Lin, SHEN Cheng-jie. Dissimilar joining of TiAl alloy and Ni-based superalloy by laser welding technology using V/Cu composite interlayer [J]. Optics and Laser Technology, 2019, 111: 205−213.
[42] WANG Jie, XIONG Qing-lian, WANG Jun, XIONG Yan-lin, YANG Jin, ZHANG Fu-qi. Microstructure and mechanical properties of YG8/IN718 alloy joints prepared by vacuum brazing [J]. Vacuum, 2019,169: 1−5.
[43] CHEN Bing-qing, XIONG Hua-ping, GUO Shao-qing, SU Bing-bing, CHEN Bo, TANG Si-yi. Microstructure and mechanical properties of dissimilar welded Ti_3Al/Ni-based superalloy joint using a Ni−Cu filler alloy [J]. Metallurgical and Materials Transactions A, 2015, 46(2): 756−761.
[44] SIMOES S, TAVARES C J, GUEDES A. Joining of γ-TiAl alloy to Ni-based superalloy using Ag−Cu sputtered coated Ti brazing filler foil [J]. Metals, 2018, 8(9): 1−14.

热等静压扩散连接 CuAgZn/GH909 接头组织及力学性能

肖 毅，郎利辉，徐文才

北京航空航天大学 机械工程及自动化学院，北京 100191

摘 要：通过热等静压−扩散连接工艺直接连接 CuAgZn 和 GH909，利用扫描电镜(SEM)、能谱仪(EDS)和 X 射线衍射仪(XRD)观察接头的显微组织和成分，并通过测试显微硬度和剪切强度研究接头的力学性能。结果表明，CuAgZn/GH909 结合界面紧密完整，接头密实、均匀，无未连接的缺陷。接头的最大显微硬度为 HV 443，高于两种基体合金，平均剪切强度高达 172 MPa。由此得出，CuAgZn 和 GH909 两种合金通过热等静压−扩散连接工艺在 700 °C、150 MPa 和 3 h 的参数下可以实现良好的冶金结合。

关键词：CuAgZn 合金；GH909 高温合金；扩散连接；热等静压

(Edited by Xiang-qun LI)